Identification of the constitutive equation by the indentation technique using plural indenters with different apex angles

Masatoshi Futakawa[a)]
Department of Nuclear Energy Systems, Japan Atomic Energy Research Institute, Tokai-mura, Naka-gun, Ibakaki-ken, 319-1195, Japan

Takashi Wakui and Yuji Tanabe
Department of Mechanical Engineering, Niigata University, Ikarashi Ni-nocho, Niigata-shi, Niigata-ken, 950-2181, Japan

Ikuo Ioka
Department of Nuclear Energy Systems, Japan Atomic Energy Research Institute, Tokai-mura, Naka-gun, Ibakaki-ken, 319-1195, Japan

(Received 8 January 2001; accepted 24 May 2001)

This paper describes a novel technique for determining the constitutive equation of elastic–plastic materials by the indentation technique using plural indenters with different apex angles. Finite element method (FEM) analyses were carried out to evaluate the effects of yield stress, work hardening coefficient, work hardening exponent, and the apex angle of indenter on the load–depth curve obtained from the indentation test. As a result, the characterized curves describing the relationship among the yield stress, work hardening coefficient, and the work hardening exponent were established. Identification of the constants of a constitutive equation was made on the basis of the relationship between the characterized curves and the hardness given by the load–depth curve. This technique was validated through experiments on Inconel 600 and aluminum alloy. The determined constitutive equation was applied to the FEM analyses to simulate the deformation including necking behavior under uniaxial tension. The analytical results are in good agreement with experimental results.

I. INTRODUCTION

The indentation technique with a depth-sensing measuring system is very promising and convenient for evaluating mechanical properties of materials at the micro- or nanometer scale level: thin surface layers, coatings, ion implanted layers, corroded surface layers, etc. A lot of effort has been made so far to examine the relationship between the indentation load versus depth curve behavior and the various fundamental mechanical properties of very thin surface areas and/or films. Some analyses using finite element method (FEM), which can treat elastic and plastic deformations, have been carried out to examine effects of interaction between the thin film and the substrate on the load/depth curve.[1–7] In particular, Bhattacharya *et al.* have developed semi-analytically functional equations of the thin film on the substrate through systematic finite element simulations to predict the hardness variation with depth under various conditions and to separate the elastic properties of the film from those of the substrate.[2] Likewise, the present authors have applied the depth-sensing indentation technique to investigate the degradation of mechanical properties of corroded surface layers of some ceramic materials.[8,9] Inverse analyses using FEM on the load/depth curve have been carried out to quantitatively evaluate the variation of mechanical properties of the corroded surface layers.[9,10]

Although various fundamental mechanical properties to describe the deformation of materials seem to be obtainable by the depth sensing indentation technique, it is still difficult to derive the constitutive equations of various materials from the information obtained from the indentation technique. Giannakopoulos *et al.* investigated in detail the influence of mechanical properties, Young's modulus, yield stress, and hardening coefficient on the deformation of materials under a Vickers indenter by using FEM analyses.[11] Field and Swain focused on the behavior of piling up and sinking in to characterize mechanical properties.[12] Milman *et al.* used indenters with different apex angles to experimentally characterize the mechanical properties of materials, by taking into account the dependence of the apex angle of indenters on

[a)]Address all correspondence to this author.
e-mail: futakawa@popsvr.tokai.jaeri.go.jp

the plastic zone size.[13] Cheng *et al.* addressed the limitation for the determination of the constitutive equation by using conical and pyramidal indenters.[14]

In this paper, we describe a novel technique for determining the constitutive equation of materials semi-experimentally through combination of experimental data obtained by indentation tests using plural indenters with the FEM analyses. The technique was then applied to a Ni-based alloy, Inconel 600, and aluminum alloy, A5056, to demonstrate its availability for the determination of their constitutive equations. The determined stress–strain curve was used to describe the deformation including necking behavior under uniaxial tension. The analytical results had good agreements with experimental ones.

II. IDENTIFICATION OF THE CONSTITUTIVE EQUATION

A. FEM analysis

The FEM analyses were carried out to systematically examine the relationship between indent load/depth curve and the constants of the constitutive equation,

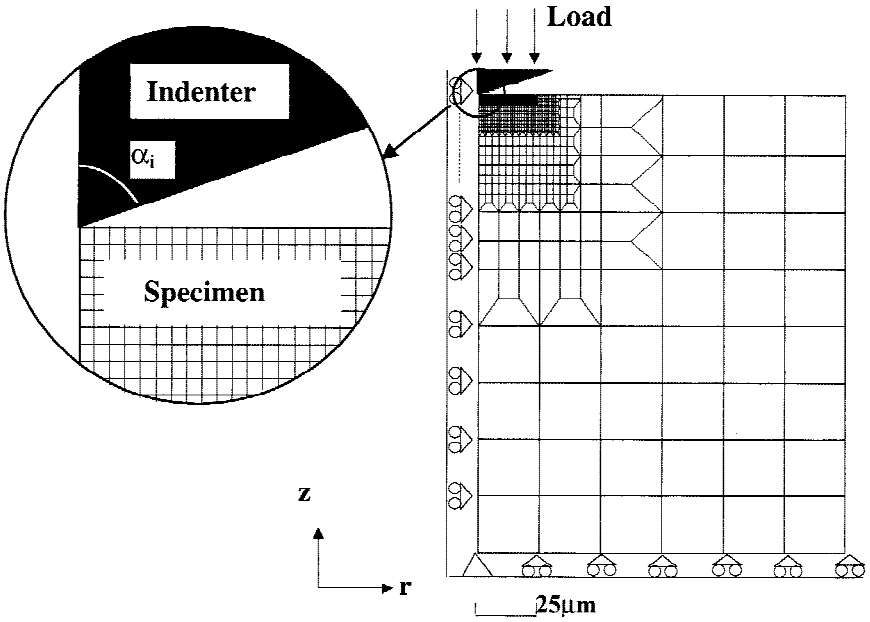

FIG. 1. Schematic illustration of FEM analysis model.

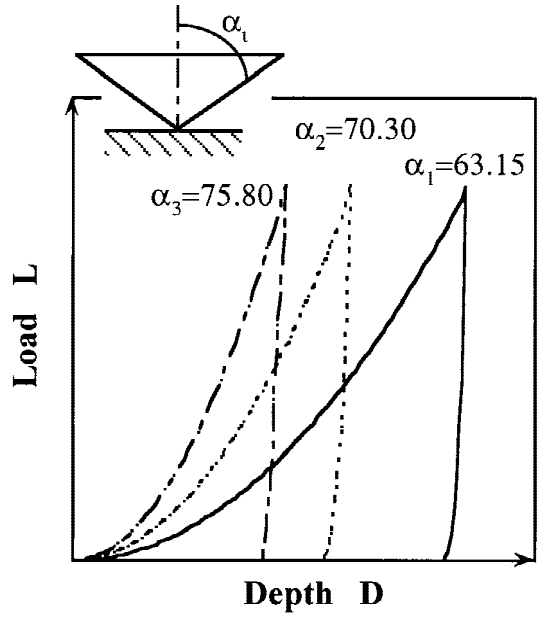

FIG. 2. Typical load–depth curves using conical indenters with different apex angles in FEM analysis.

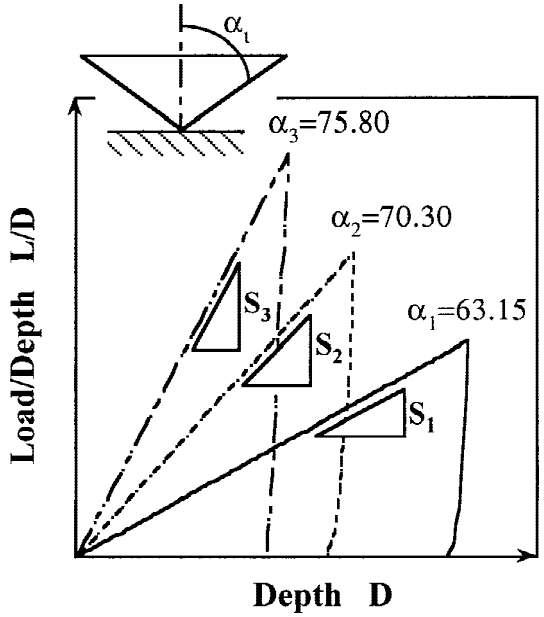

FIG. 3. Load/depth–depth curves using conical indenters with different apex angles in FEM analysis.

using an explicit FEM code, LS-DYNA,[15] which enables us to robustly analyze a large deformation accompanying with contacting behavior. In this analysis, the indenter and specimen were treated as axisymmetric two-dimensional bodies to take calculative efficiency into account. The model is schematically illustrated in Fig. 1. The indenter used in the experiment was modeled to be conical. The apex angle of indenter was determined by taking account of geometrical similitude between indenters in the experiment and analysis. That is, because of the geometrical similitude, the projected area A_p at the penetrated depth D_p is related to the D_p by

$$A_p = gD_p^2 \quad , \tag{1}$$

where g is the geometrical factor of the indenter.[16] The g-values are 24.5 for Vickers and Berkovich indenters. The apex angle of the conical indenter with the same g-value, 24.5, as a Vickers indenter becomes 70.30°. Although the discrepancy between the axisymmetric two-dimensional and the inherent three-dimensional models is enhanced on the deformation of a few elements adjacent to the indenter edges, it is not expected to cause any noticeable difference in the load–depth relationship. The modeled indenter was perfectly rigid. The contact interface between the specimen and the indenter tip was assumed to be frictionless, because throughout preliminary calculations the frictional force induced with friction coefficients up to 0.3 had few effects on the load–depth relationship. The mesh size was given to be sufficiently fine to keep accuracy: the minimum element size around an apex contacting zone was 0.05 μm. The total number of the elements used in the model was 1509. The loading rate in the calculation was small enough to neglect an inertia effect as a static condition.

The constitutive equation of the material was assumed to be a simple power law which is generally believed to be applicable to normal metallic materials as follows:

$$\sigma = E\epsilon \quad \sigma \leqslant \sigma_y \quad , \tag{2}$$

$$\sigma = A(\epsilon_0 + \epsilon)^n \quad , \tag{3}$$

$$\epsilon_0 = (\sigma_y/A)^{1/n} - (\sigma_y/E) \quad \sigma > \sigma_y \quad , \tag{4}$$

where σ is true stress, ϵ true strain, E Young's modulus, σ_y yield stress, A work hardening coefficient, and n work hardening exponent.

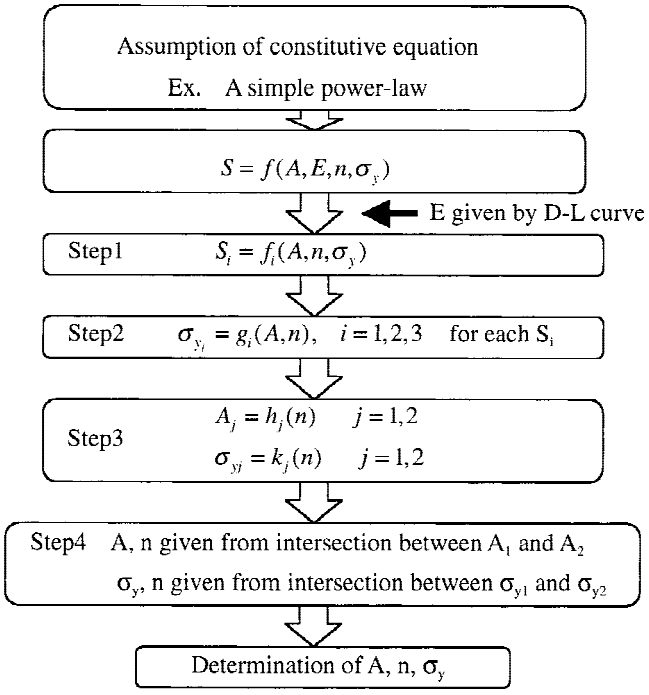

FIG. 4. Flow chart of the methodology for determining the parameter values in the given constitutive equation.

TABLE I. σ_y, A, and n values used to systematically and numerically examine the relationship among σ_y, A, and n, and the S-value; $S = f(A, n, \sigma_y)$.

σ_y (MPa)	200, 400, 600, 800
A (MPa)	200, 400, 600, 800, 1000, 1200, 1400, 1600
n	0.2, 0.3, 0.4, 0.5, 0.6, 0.7, 0.8

B. Flow for determining constants of the constitutive equation

Basically we consider that the number of the indenters with different apex angles should be equal to the number of unknown constants in the constitutive model to determine the values of the constants. For example, as long as

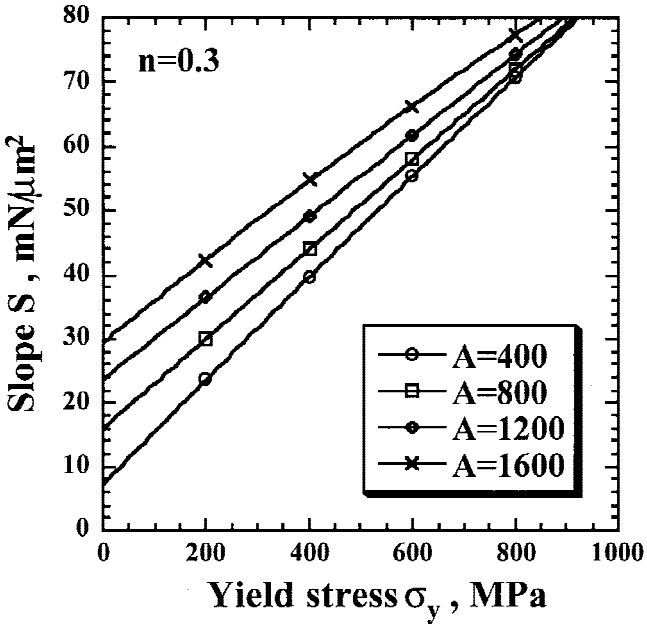

FIG. 5. $S = f(A, n, \sigma_y)$ at $n = 0.3$ with respect to the A-value.

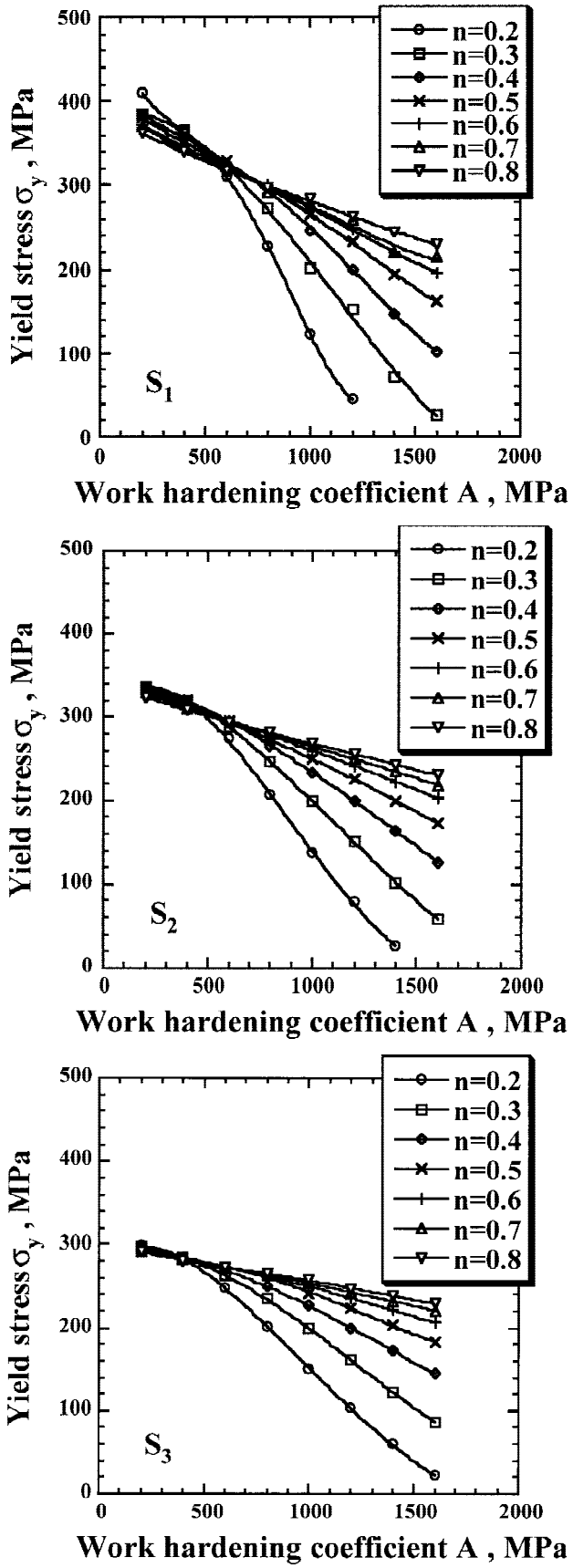

FIG. 6. Relationship among the A-value, n, and σ_y-value for $S_{1,2,3}$.

we describe the deformation of certain materials under imposed stresses by using the assumed constitutive equation, Eqs. (2)–(4), it is necessary to determine the four constants. The number of different indenters should be the same as the number of the unknown constants at least, as mentioned above. Nevertheless, Young's modulus E can be given from the unload–depth curve directly, using the following equation:[17]

$$\frac{E}{1-\nu^2} = \frac{1}{2}\sqrt{\frac{\pi}{c_i h_p{}^2}\frac{\mathrm{d}p}{\mathrm{d}h}} \quad , \tag{5}$$

where ν is Poisson's ratio, $\mathrm{d}p/\mathrm{d}h$ and h_p are the initial slope during unloading and the intersection value of the depth axis (at $P = 0$), and c_i is a constant dependent on

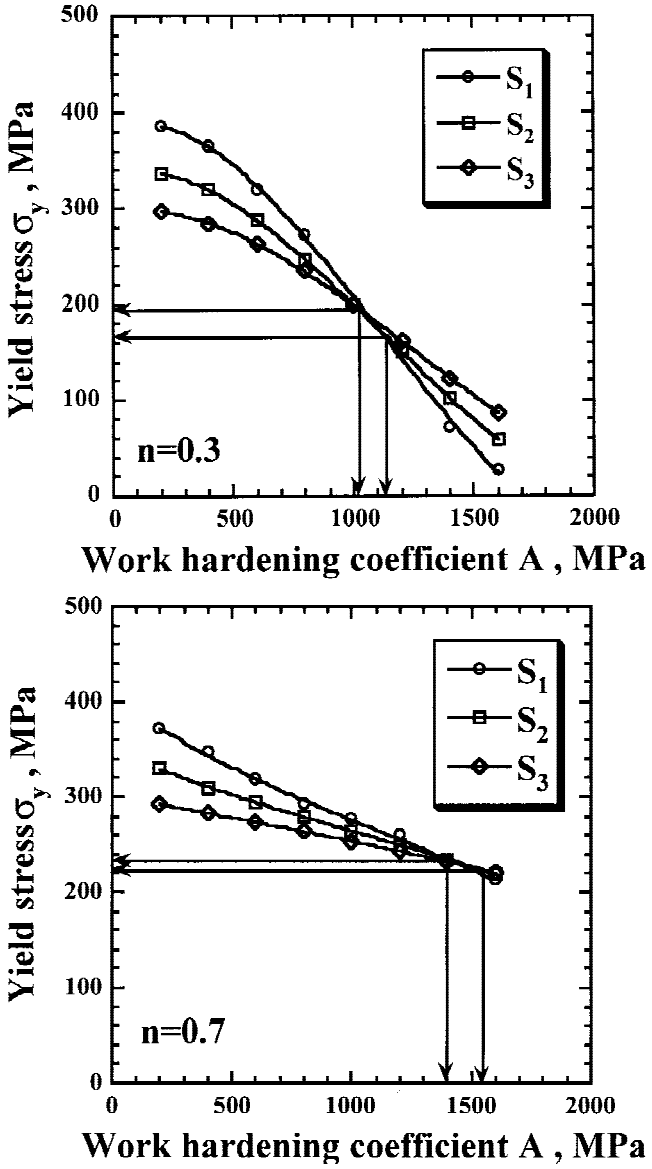

FIG. 7. Dependency of $\sigma_y = g(A, n)$ on the S-values for the n-values of 0.3 and 0.7.

the apex angle; e.g., $c_i = 24.5$ for the Vickers and Berkovich indenters. As a result, the number of the unknown constants we should determine is reduced to three, i.e., σ_y, A, and n in Eqs. (2)–(4).

On the basis of the FEM analysis, the schematic drawing of load/depth curves obtained by using indenters with different apex angles is illustrated in Fig. 2. The apex angles, $\alpha_{1,2,3} = 63.2°$, 70.3°, and 75.8°, corresponds to the g-values of 12.5, 24.5, and 49.0, respectively. The load/depth curves are strongly dependent on the apex angle. Results in Fig. 2 are replotted to describe the hardness variation with the depth by using the load/depth and depth curve, L/D–D curve, as shown in Fig. 3. The slopes of the L/D–D curve during loading, $S_{1,2,3}$, are associated with the hardness. In the case of homogeneous materials having a smooth surface without any hardness distribution and any residual stress distribution in the depth direction, the S-value is theoretically independent of the depth but dependent on the apex angle of the indenter and the inherent hardness of materials.

To determine the three values of unknown constants in Eqs. (2)–(4), the three different indenters were prepared in experiments, i.e., trigonal pyramid indenters with the g-values of 12.5, 24.5, and 49.0, which have the angles between ridge lines of 111°, 115°, and 117°, and hereafter these trigonal pyramid indenters are called I_1, I_2, and I_3. We used the trigonal pyramid indenters in experiments although we used the conical indenters in the analyses, because the trigonal pyramid indenter with a sharp apex is more readily and precisely manufactured than the conical indenter. The trigonal pyramid indenter with the g-value of 24.5 corresponds to the Berkovich indenter. During loading the L/D–D curves increase almost linearly with depth, and the S-values are dependent on the apex angle. The S-value is associated with the hardness that is believed to be an inherent value of the material and reflects the mechanical properties.[18]

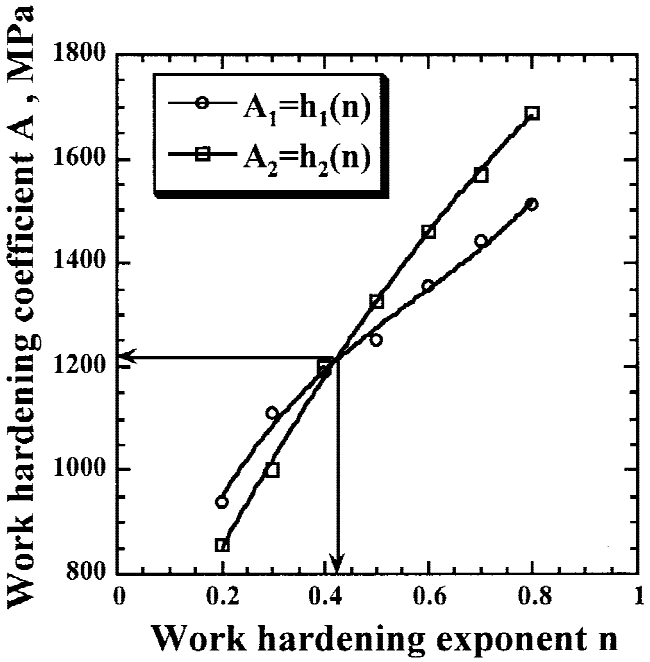

FIG. 8. Relationship between A and n: $A_i = h_i(n)$.

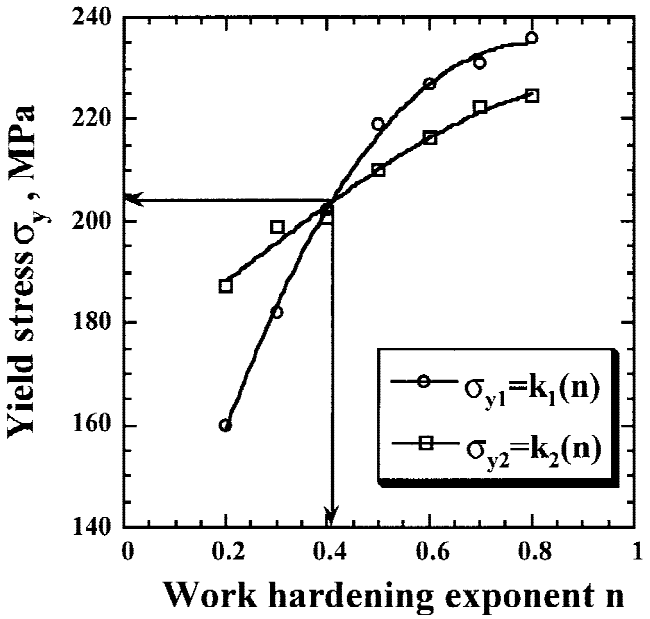

FIG. 9. Relationship between σ_y and n: $\sigma_y = k(n)$.

TABLE II. Chemical compositions of tested materials (mass%).

(a) Inconel 600

Ni	Cr	Fe	Mn	C
>72	14–17	6–10	<1	<0.15

(c) A5056

Si	Fe	Cu	Mn	Mg	Cr	Zn	Al
<0.30	<0.40	<0.10	0.05–0.20	4.5–5.6	0.05–0.20	<0.10	Bal.

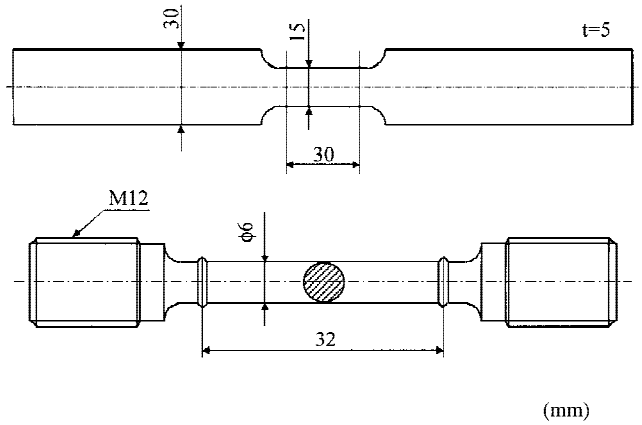

FIG. 10. Dimensions of specimens.

The constants of the pre-assumed constitutive model are determined on the basis of the relationship among σ_y, A, n, and the S-value. Figure 4 shows the flow chart of the methodology for determining A, n and σ_y. First an appropriate constitutive equation should be assumed, i.e., the simple power-law equation described by Eqs. (2)–(4). The S-value is given as a function of A, E, n, and σ_y.

TABLE III. Slopes and Young's moduli evaluated for Inconel 600 and A5056.[a]

	S_1 (mN/μm^2)	S_2 (mN/μm^2)	S_3 (mN/μm^2)	E (GPa)
Inconel 600	27.09 (1.31)	47.94 (4.37)	84.05 (5.03)	163 (5.4)
A5056	9.91 (0.50)	18.60 (1.36)	33.60 (2.30)	68 (9.3)

[a]Deviations in parentheses.

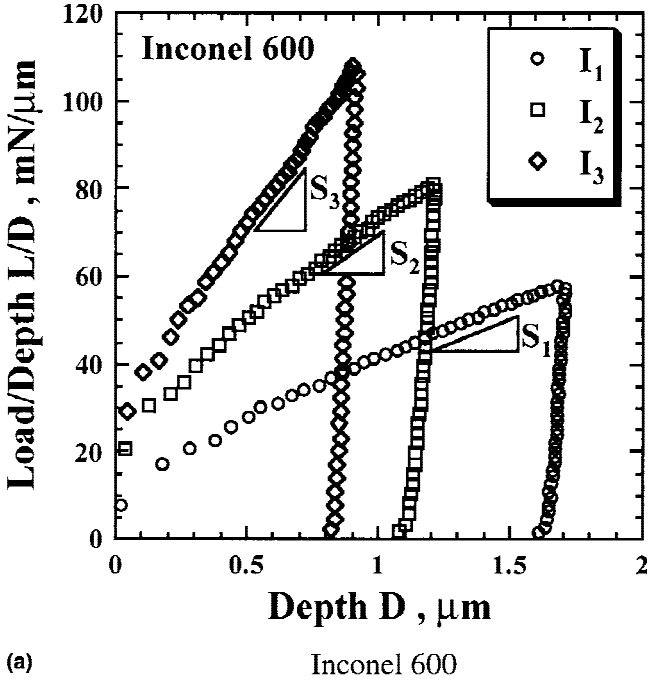

(a) Inconel 600

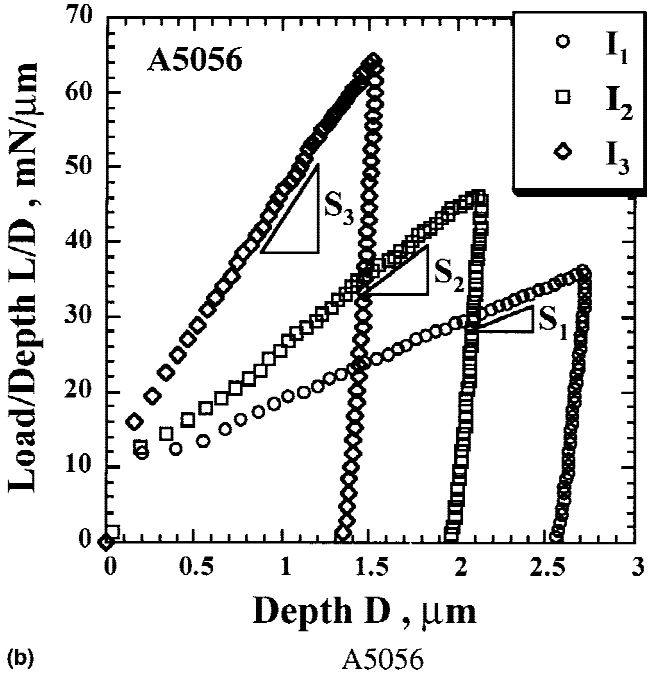

(b) A5056

FIG. 11. L/D–D curves measured using the trigonal pyramid indenters, I_1, I_2, and I_3: (a) Inconel 600; (b) A5056.

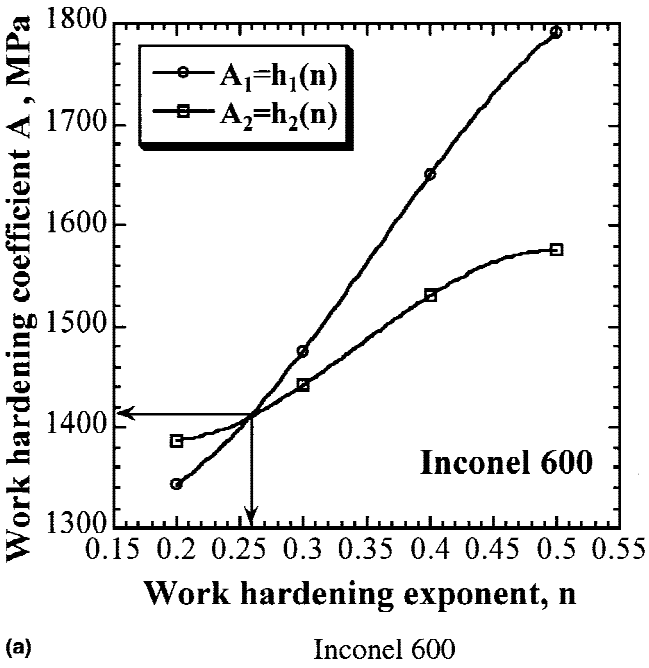

(a) Inconel 600

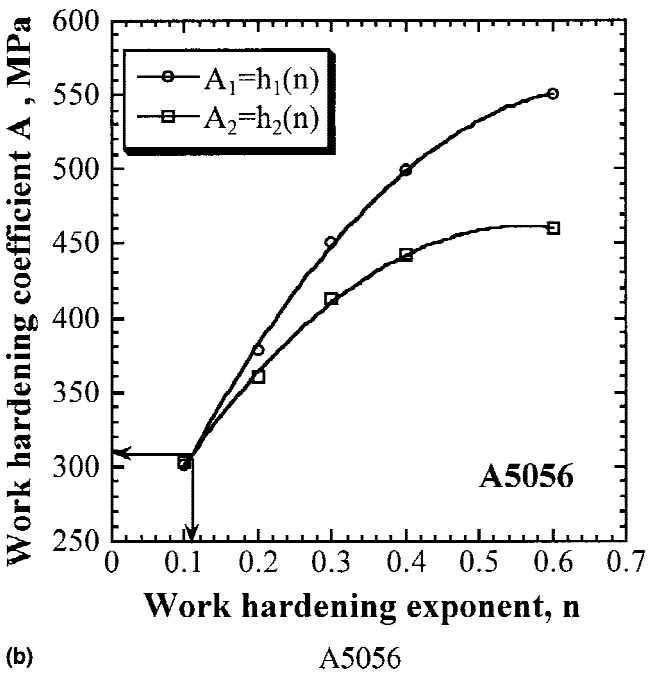

(b) A5056

FIG. 12. Relationships between work hardening exponent n and work hardening coefficient A: (a) Inconel 600; (b) A5056.

Young's modulus E is obtained from the load–depth curve.

In step 1, the relationship among σ_y, A, n, and the S-value, $S = f(A, n, \sigma_y)$, was obtained numerically and systematically by using appropriate values as listed in Table I. Figure 5 shows the example of $S = f(A, n, \sigma_y)$ at $n = 0.3$ for various values of A using the conical indenter with apex angle of 70.3°. Such a relationship should be obtained for each indenter.

From these relationships, in step 2, the relationships among A, n, σ_y are given for S_1, S_2, and S_3 that are the S-values experimentally obtained using the trigonal pyramid indenters, I_1, I_2, and I_3, as shown in Fig. 6. The results shown in Fig. 6 are replotted to describe the dependency of $\sigma_y = g(A, n)$ on the S-value for each n-value and to obtain the intersection between the S_1 and the S_2 curves as well as between the S_2 and the S_3 curves. For example, the results of $n = 0.3$ and 0.7 are plotted in Fig. 7.

From these relationships obtained for each n-value, in step 3, the correlations between A and n, i.e., $A = h(n)$, and between σ_y and n, i.e., $\sigma_y = k(n)$, are obtained as shown in Figs. 8 and 9.

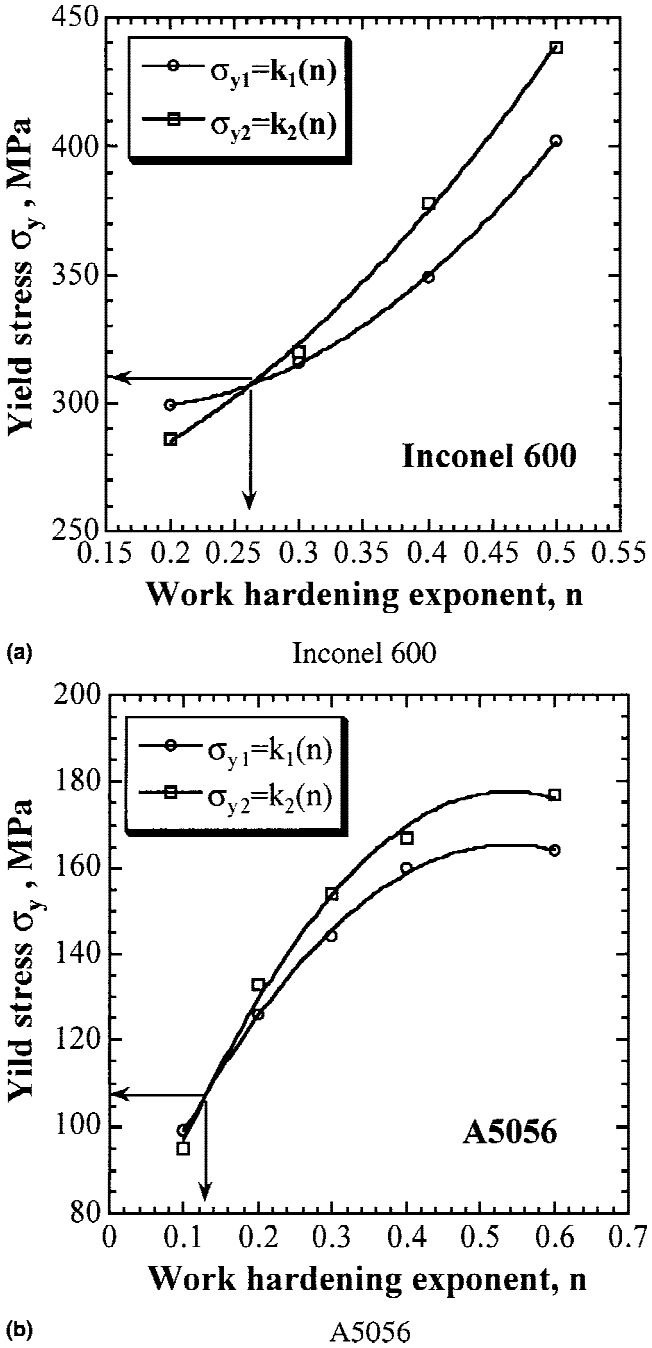

FIG. 13. Relationships between work hardening exponent n and yield stress σ_y: (a) Inconel 600; (b) A5056.

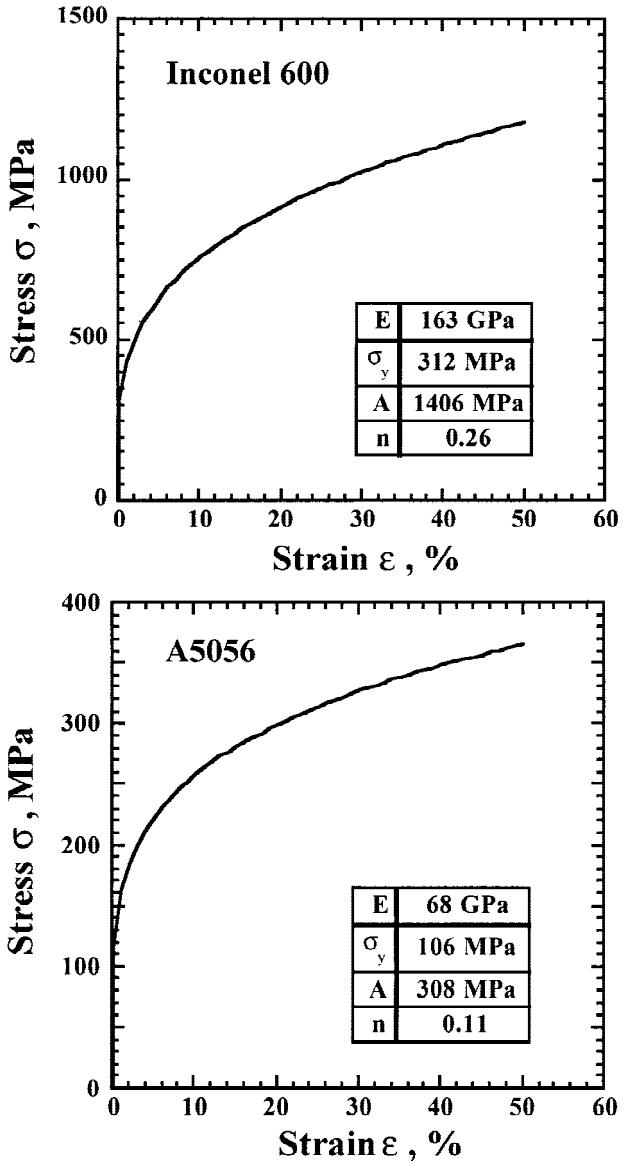

FIG. 14. True stress–strain curves determined for Inconel 600 and A5056.

In the step 4, A, n, and σ_y are determined from the values at the intersection between two curves, respectively. Through these steps, we can identify the constitutive equation of the materials.

III. EXPERIMENTAL METHOD

A. Indentation test

The method developed in Sec. 2 was applied to two kinds of materials, i.e., nickel-based alloy, Inconel 600, and aluminum alloy, A5056. The chemical compositions of both materials are shown in Table II. The specimens of $15 \times 30 \times 5$ mm^3 were polished at a 600-grit finish for the indentation test. The indentation tests were carried out on polished surfaces of the specimens at room temperature using the trigonal pyramid indenters, I_1, I_2, and I_3. A testing machine, DUH-201 (Shimadzu Co., Japan), was used for the test. A load was imposed through the indenter on the specimen's surface with a loading rate of 2.7 mN/s, held for 1 s, and then removed. A suitable maximum load was chosen as taking account of the size effect[19] mainly due to the roundness of the indenter apex and the roughness of the specimen surface. Since the hardness of the specimens was almost constant at loads greater than 50 mN, the load of 50 mN at minimum was applied to neglect influences due to the surface condition of materials and the roundness of the indenter apex. During loading and unloading, the load and the indent depth were continuously measured with a resolution of 19.6 μN and 1 nm, respectively.

B. Uniaxial tensile test

The uniaxial tensile tests were carried out at room temperature. Figure 10 illustrates dimensions of the specimens, which are the rod type for the Inconel 600 and the plate type for the A5056. The elongation of the specimen was measured at the crosshead. The tensile loads were applied at the crosshead speeds of 2.25 mm/min for Inconel 600 and at 0.2 mm/min for A5056.

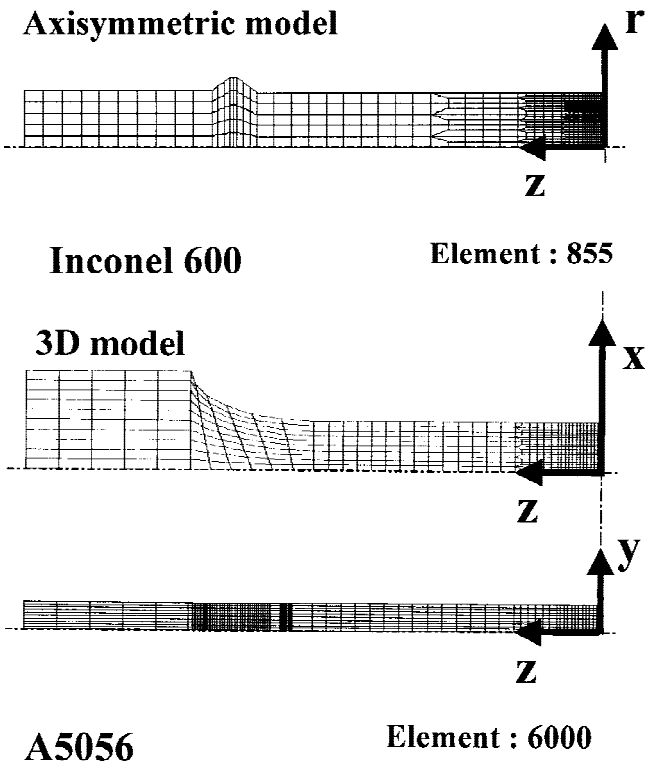

FIG. 15. FEM models for uniaxial tensile specimens.

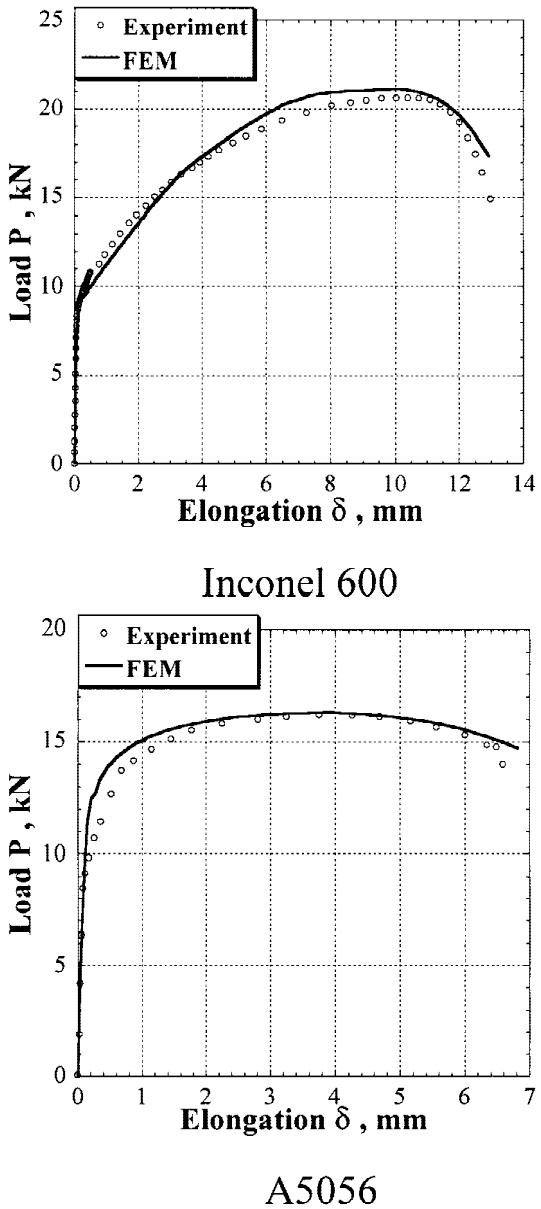

FIG. 16. Comparison between experimental and analytical elongation–load curves.

IV. VALIDATION OF THE METHOD

Figure 11 shows the *L*/*D*–*D* curves measured for Inconel 600 and A5056 using the trigonal pyramid indenters, I_1, I_2, and I_3. During loading, except for early stages of small loads, the slopes of S_1, S_2, and S_3 were almost constant, independent of the indentation load. The values of the slopes S_1, S_2, and S_3 and Young's moduli E evaluated by Eq. (3) for Inconel 600 and A5056 are listed in Table III. Regardless of the apex angles of indenters, each corresponding slope of A5056 is smaller than that of Inconel 600. Since the slope is equivalent to the hardness, Inconel 600 can be said to be harder than A5056.

According to the method described in the Sec. 2, the relationships between work hardening exponent n and work hardening coefficient A and between hardening exponent n and yield stress σ_y were obtained using the slopes S_1, S_2, and S_3 and Young's moduli in Table III, as shown in Figs. 12 and 13. We determined the values of A, n, and σ_y from the intersections between A_1 and A_2 curves and between σ_{y1} and σ_{y2} curves. The true stress–strain curves determined for Inconel 600 and A5056 are shown in Fig. 14. The values of E, σ_y, A, and n are listed in Fig. 14.

To validate the identified constitutive model, uniaxial tensile tests were carried out. The prediction for the local deformation followed by ductile failure was very sensitive to the constitutive equation.[20] The constitutive equations identified for Inconel 600 and A5056 were used for the FEM analysis as illustrated in Fig. 15. A two-dimensional axisymmetric model for Inconel 600 and a quarter model for A5056 have a high mesh density around a center of the specimen. The deformation of the specimen was calculated by LS-DYNA.[15] Loading of the specimen was simulated by moving the upper end of the model at constant velocities, which were equivalent to the experimental conditions for Inconel 600 and A5056. Figure 16 shows the comparison between experimental and analytical results on the elongation–load curves. Figure 17 shows the failure deformation of the specimen compared with the analytical results at failure elongation. Despite the kinds of materials, good agreements are given between them on both the elongation–load curves and the failure deformation. It was found from Figs. 16 and 17 that the analytical results are representable well to the actual necking behavior and that the presented technique based on the indentation tests could be applied to find out optimum parameter values in the given constitutive equation.

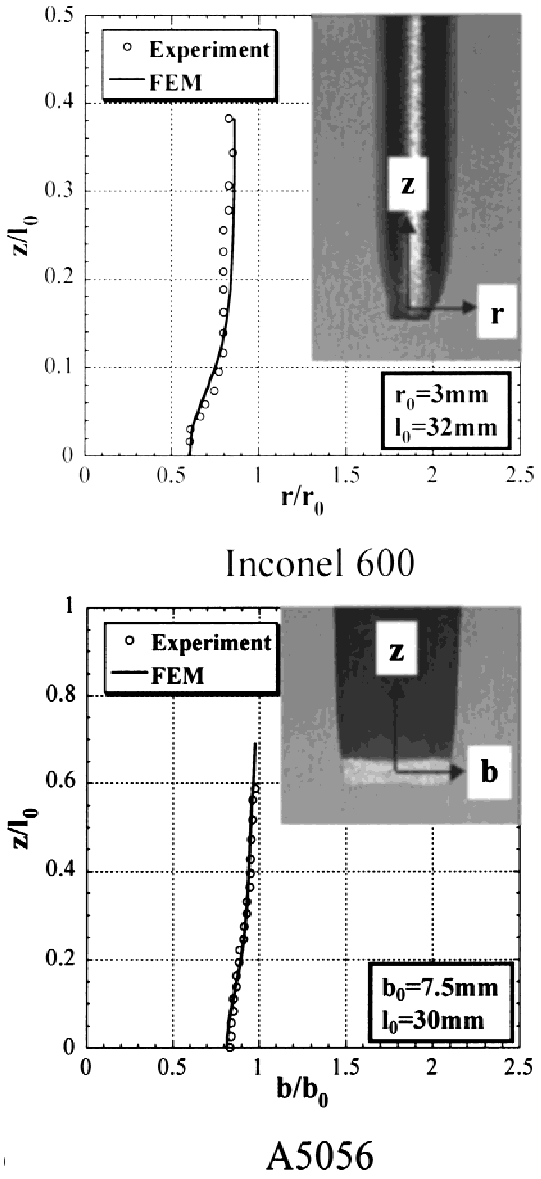

FIG. 17. Comparison between experimental and analytical results for necking behavior under uniaxial tension.

V. CONCLUSION

A novel technique for identification of the constitutive equation has been developed. This technique is established on the basis of the indentation test using plural indenters with different apex angles combined with FEM analyses. The constitutive equations were applied to the FEM analyses to describe uniaxial tensile deformations of two materials, nickel-based alloy, Inconel 600, and aluminium alloy, A5056. The analytical results using the identified constitutive equation well predicted the actual deformations with the inclusion of necking behavior under uniaxial tension. It was concluded that the technique based on the indentation test with plural indenters could be applied to identify the constitutive equation for materials.

ACKNOWLEDGMENTS

The authors thank Dr. Kurata of the Japan Atomic Energy Institute and Prof. Date of Tohoku Gakuin University for the tensile tests and Mr. Suzuki of the Japan Atomic Energy Institute for polishing specimens.

REFERENCES

1. A.K. Bhattacharya and W.D. Nix, Int. J. Solids Struct. **24,** 881 (1988).
2. A.K. Bhattacharya and W.D. Nix, Int. J. Solids Struct. **24,** 1287 (1988).
3. T.A. Lausen and J.C. Simo, J. Mater. Res. **7,** 618 (1992).
4. E.R. Kral, K. Komvopoulos, and D.B. Bogy, ASME J. Appl. Mech. **62,** 20 (1995).
5. E.R. Kral, K. Komvopoulos, and D.B. Bogy, ASME J. Appl. Mech. **62,** 29 (1995).
6. G. Care and A.C. Fischer-Cripps, J. Mater. Sci. **32,** 5653 (1997).
7. N. Huber and Ch. Tsakmakis, J. Eng. Mater. Tech. ASME **120,** 143 (1998).
8. N. Nishiyama, M. Futakawa, I. Ioka, K. Onuki, S. Shimizu, M. Eto, T. Oku, and M. Kurabe, J. Soc. Mater. Sci. Jpn. **48,** 746 (1999) (in Japanese).
9. M. Futakawa, T. Wakui, I. Ioka, and M. Eto, J. Eur. Ceram. Soc. **20,** 143 (1998).
10. T. Wakui, M. Futakawa, Y. Tanabe, and M. Eto, J. JSME-A **65,** 2399 (1999) (in Japanese).
11. A.E. Giannakopoulos, P.L. Larsson, and R. Vestergaard, Int. J. Solids Struct. **31,** 2679 (1994).
12. J.S. Field and M.V. Swain, J. Mater. Res. **10,** 101 (1995).
13. Yu.V. Milman, S.I. Chugunova, I.V. Goncharova, and S. Luyckx, Sci. Sintering **29,** 155 (1997).
14. Y. Cheng and C. Cheng, J. Mater. Res. **14,** 3493 (1999).
15. *LS-DYNA USER'S MANUAL,* (Livermore Software Technology Corporation, 1995).
16. M. Sakai, S. Shimizu, and T. Ishikawa, J. Mater. Res. **14,** 1 (1999).
17. M.F. Doerner and W.D. Nix, J. Mater. Res. **1,** 601 (1986).
18. M. Inamura and T. Suzuki, Seisankenkyu **42,** 257 (1990) (in Japanese).
19. P.M. Sargent, In *Microindentation Techniques in Materials Science and Engineering,* ASTM STP 889, edited by P.J. Blau and B.R. Lawn (ASTM, West Conshohocken, PA, 1986), pp. 160–174.
20. M. Futakawa and N. Butler, Eng. Fract. Mech. **54,** 349 (1996).